ELSEVIER

Contents lists available at ScienceDirect

# Weather and Climate Extremes

journal homepage: www.elsevier.com/locate/wace





# Temporal changes in dependence between compound coastal and inland flooding drivers around the contiguous United States coastline

Ahmed A. Nasr<sup>a,\*</sup>, Thomas Wahl<sup>a</sup>, Md Mamunur Rashid<sup>b,a</sup>, Robert A. Jane<sup>a</sup>, Paula Camus<sup>c</sup>, Ivan D. Haigh<sup>c</sup>

- <sup>a</sup> Civil, Environmental, And Construction Engineering & National Center for Integrated Coastal Research, University of Central Florida, 12800 Pegasus Drive, Suite 211, Orlando, FL, 32816-2450, USA
- <sup>b</sup> Division of Coastal Sciences, School of Ocean Science and Engineering, Ocean Springs, MS, 39564, USA
- <sup>c</sup> School of Ocean and Earth Science, National Oceanography Centre Southampton, University of Southampton, Waterfront Campus, European Way, Southampton, SO14 3ZH. UK

#### ARTICLE INFO

Keywords:
Compound flooding
Copula
Dependence
Flood risk
Temporal changes
United States

#### ABSTRACT

Flooding in low-lying coastal zones arises from coastal (storm surge, tides, and waves), fluvial (excessive river discharge), and pluvial (excessive surface runoff) drivers. We analyse changes in compound flooding potential around the contiguous United States (CONUS) coastline stemming from select combinations of these flooding drivers using long observational records with at least 55 years of data. We assess temporal changes in the tail (extremal) dependence (y) using a 30-year sliding time window. Periods of strong tail dependence are found for the windows centered between the 1960s and 1980s/1990s at several locations for surge-discharge (S-Q) and surge-precipitation (S-P) combinations. Changes in dependence are associated with large-scale climate indices such as the Arctic Oscillation (AO) and El Nino Southern Oscillation indices (Niño 1.2 and Niño 3), among others. The significance of potential changes in the dependence structure is subsequently tested using Kullback-Leibler (KL) divergence. We find that changes are mostly not significant. Finally, we perform a complete multivariate statistical analysis exemplarily for one selected pair of variables at one location (S-Q in Washington, DC), allowing for varying dependence strength and structure as well as changes in the marginal distributions. Combined changes with increase in the dependence and marginals exacerbate the predicted compound flood potential. The comprehensive analysis presented here provides new insights into how and where compound flooding potential has changed with time, demonstrates associated links with large-scale climate indices, and highlights the effects of changes in the dependence and marginals in a multivariate statistical framework.

## 1. Introduction

Floods are among the most costly and dangerous natural catastrophes, especially in coastal locations that are densely populated and have high socioeconomic importance (Hanson et al., 2011). In the contiguous United States (CONUS), 40% of the population resides in coastal counties, and 40% of them are exposed to coastal hazards (NOAA Office for Coastal Management). In total, 66% of U.S. losses from weather and climate extremes between 1980 and 2020 were due to inland floods and tropical cyclones causing storm surges, waves, wind, and extreme precipitation (Smith, 2020).

In coastal areas, flooding can occur from multiple hydrometeorological drivers such as coastal drivers including storm surges

and waves (coastal/oceanographic), and inland drivers such as excessive river discharge (fluvial), and direct runoff due to extreme precipitation (pluvial). Flood-related impacts can be exacerbated, depending on local conditions, when two or more of these drivers occur at the same time (concurrently) or when separated by a short period, such as a few hours or days (successively) (Zscheischler et al., 2018, 2020). Traditionally, past flood risk assessments accounted for individual drivers and falsely assumed independence between them, which can lead to an underestimation of flood risk, especially for coastal communities (Wahl et al., 2015).

Over the past decade, assessments of the potential for compound inland and coastal flooding drivers to co-occur have been undertaken at the global scale (e.g., Ward et al., 2018; Couasnon et al., 2020), regional

E-mail address: Ahmed.Nasr@ucf.edu (A.A. Nasr).

<sup>\*</sup> Corresponding author.

scale (e.g., Wahl et al., 2015; Moftakhari et al., 2017; Paprotny et al., 2020; Hendry et al., 2019; Camus et al., 2021; Nasr et al., 2021), and for local case studies (e.g., Kew et al., 2013; Rueda et al., 2016; Bevacqua et al., 2017; Couasnon et al., 2018; Jane et al., 2020, 2022; Kim et al., 2022; Peña et al., 2023; Santos et al., 2021b). Santos et al. (2021a) performed a compound analysis between surge and precipitation in a managed water system using a large ensemble of model data to study internal climate vriability. Challenges in analysing compound events are often related to the availability of longer observation records, in particular overlapping records which are required for a dependence analysis, which are limited (e.g., Jane et al., 2022; Santos et al., 2021b). To overcome this challenge, model/reanalysis data can be used instead (e.g., Marcos et al., 2019; Bevacqua et al., 2020; Couasnon et al., 2020; Camus et al., 2021). However, results from models should be interpreted with care as dependence could be overestimated or underestimated depending on the pairs of variables, as shown by Nasr et al. (2021). Thus, long overlapping records of observations are favoured to assess temporal changes in bivariate time series (e.g., Wahl et al., 2015) without introducing additional uncertainty from models (Nasr et al.,

Climate change affects variables/drivers of compound flooding (e.g., Camelo et al., 2020 and Tabari, 2020). While there are many studies that investigate effects of climate change on individual flooding drivers, few studies focused on the non-stationary interaction between those drivers over time. Wahl et al. (2015) analysed dependence between storm surge and precipitation at several coastal locations around the CONUS using Kendall's rank correlation coefficient  $(\tau)$  calculated on conditional samples (two-way sampling) by applying a sliding time window. They found that the dependence between storm surge and precipitation had changed over time at many of the locations analysed.

Moftakhari et al. (2017) studied compounding effects of fluvial floods and sea level rise at select locations in the U.S. and concluded that non-stationarity in coastal water levels due to sea-level rise (change in the marginal distribution) increases flood risk. Naseri and Hummel (2022) studied dependence between annual maximum precipitation and coincident sea-level. They found that sea-level rise and dependence have significant effects on joint return periods. Using numerical models, Gori et al. (2022) found that by 2 100 the frequency of joint extreme surge and rainfall could increase by 7-36-fold in the southern U.S. and by 30-195-fold in the northeast U.S. due to decreasing translation spend and increasing storm intensity of tropical cyclones.

Earlier studies have shown links between coastal flooding drivers and large-scale climate variability (e.g., Rashid and Wahl, 2020). This poses the question whether dependence between those drivers could also be linked to large-scale climate indices. Variability in extreme sea-levels along the U.S. coastlines, for example, was found to be linked to large-scale climatic indices at different time scales (e.g., Wahl and Chambers, 2016; Rashid and Wahl, 2020). El-Niño Southern Oscillation (ENSO) and indices derived from it (e.g., Southern Oscillation Index (SOI), Pacific Decadal Oscillation (PDO), North Pacific Index (NPI), Multivariate ENSO Index, Niño 2.1, and Niño 3.1) influence storm surge, which is the meteorological component of sea-level, along the U.S. west coast (e.g., Bromirski et al., 2003, 2017; Serafin and Ruggiero, 2014; Wahl and Chambers, 2016; Rashid and Wahl, 2020). ENSO was also linked to tropical cyclone activity in the Gulf of Mexico and Atlantic (Kennedy et al., 2007) which affects storm surge and precipitation (cascading to pluvial and fluvial floods) in the south-eastern U.S.

Here we extend previous studies (particularly Nasr et al., 2021; Wahl et al., 2015) and carry out a continental-scale analysis of the temporal changes/variability in compound flooding potential caused by oceanographic (storm surge), fluvial (excessive river discharge), and pluvial (direct surface runoff from precipitation) sources using observational data. We have four key objectives. Our first objective is to characterize and map the change in dependence strength between inland and coastal drivers at locations with long overlapping records (at least 55 years of data) around the CONUS coastline. We perform this analysis for the

whole year and after splitting the time series into seasons (or half years): tropical (June–November) and extra-tropical (December–May). This will show where and when compound flooding potential varied due to changes in dependence strength, and if these changes are more pronounced in one season compared to the other. Our second objective is to investigate whether a statistically significant link exists between time-varying dependence strength and large-scale climate indices. This will allow physical interpretation of the identified variations in the dependence strength. Our third objective is to compare the dependence structures (in addition to strength) of different combinations of flooding drivers over time. As our fourth and final objective, we demonstrate, exemplarily at one location, the effects of changes in dependence strength, structure, and marginal distributions on compound flood risk potential in a multivariate statistical framework.

The paper is structured as follows. The datasets and methods are detailed in Sect. 2. The results are presented in Sect. 3, and findings are discussed in Sect. 4. Finally, conclusions are given in Sect. 5.

## 2. Data and methods

#### 2.1. Data

We use observational data from various sources for coastal locations around the CONUS coastline. The three flood generating variables considered here are storm surge (S), river discharge (Q), and precipitation (P). In the following we provide a brief overview of data, for more details on the data and pre-processing steps we refer to Nasr et al. (2021) where the same database was used.

Hourly sea level data is available from the National Oceanic and Atmospheric Administration (NOAA; http://tidesandcurrents.noaa. gov/) database. Hourly sea-level values are detrended to eliminate mean sea-level rise. Then, we use the Unified Tidal Analysis and Prediction (UTide) package in MATLAB to perform a year-by-year harmonic tidal analysis to obtain tidal constituents (Codiga, 2011). Hourly storm surge, the meteorological component of water level of interest in this study, is represented by the non-tidal residual which is obtained by subtracting predicted tides from detrended hourly water levels. Finally, we extract daily maxima surge values from the hourly storm surge record. Daily average river discharge time series were obtained from the United States Geological Survey (USGS) National Water Information System (NWIS) (https://waterdata.usgs.gov/nwis). Cumulative daily precipitation depths were obtained from the Global Historical Climatology Network Daily (GHCN-D) hosted by NOAA's National Centers for Environmental Information (NOAA-NCEI) (https://www.ncdc.noaa.go v/ghcnd-data-access). All locations for which these data sets were obtained are shown in Fig. 1. As we are interested in investigating temporal changes, we focus on sites and pairs where the number of years of overlapping records between each pair is at least 55 years (Table S1). Applying this criterion results in omitting waves from the analysis, which were included in Nasr et al. (2021). Since we are interested in compound coastal-inland flooding drivers, the pairs considered are surge and discharge (S-Q) and surge and precipitation (S-P). From the 35 locations considered in Nasr et al. (2021), Site 12- Annapolis, MD, is excluded as it does not have 55 years of overlapping data for either S-Q or S-P.

In addition, we use the following eight climate indices, that were shown in earlier studies (e.g., Wahl and Chambers, 2016; Rashid and Wahl, 2020) to affect storm surge variability along the U.S. coast: Atlantic Multi-decadal Oscillation (AMO), Arctic Oscillation (AO), North Atlantic Oscillation (NAO), Niño 1.2 (N12), Niño 3 (N3), North Pacific Index (NPI), Pacific Decadal Oscillation (PDO), and Southern Oscillation Index (SOI). These indices represent sea-level pressure (SLP) and sea surface temperature (SST) anomalies at various spatial domains and were obtained from NOAA Physical Science Laboratory (https://psl.noaa.gov/gcos\_wgsp/Timeseries/).



Fig. 1. Selected study sites based on tide gauge data availability and at least 55 years of overlapping records between surge and discharge (S-Q) or surge and precipitation (S-P). Sites are separated into east coast, Gulf coast, and west coast locations following Nasr et al. (2021).

#### 2.2. Changes in dependence strength over time

Our first objective is to characterize and map the change in dependence strength between different drivers at locations around the CONUS coastline with long overlapping records. Here we focus on two combinations of variables with the potential for coastal-inland compound flooding.

The metric that we use to quantify dependence strength is the tail dependence coefficient ( $\chi$ ). In this method, extremal (or tail) dependence falls into two categories: (1) asymptotic tail dependence; or (2) asymptotic tail independence (Ledford and Tawn, 1997). Suppose (A, B) are a pair of variables with cumulative distribution functions ( $F_a$ ,  $F_b$ ) transformed to unit scale (0,1), (U =  $F_a$  (A), V =  $F_b$  (B)). Then, (A, B) are asymptotically tail dependent if

$$\chi = \lim_{q \to 1} P\left(F_a(A) > q | F_b(B) > q\right) \varepsilon (0, 1]$$

and asymptotically tail independent if  $\chi=0$ .  $\chi$  represents the probability of one variable being extreme (exceeding a threshold q) given that the other variable is extreme (exceeding the same threshold q). Following Nasr et al. (2021), we choose q=0.9 (90th percentile). We use the function 'taildep' from the R package extRemes (Gilleland and Katz, 2016) to calculate  $\chi$ . The significance of the calculated  $\chi$  values is estimated using a bootstrap method following Svensson and Jones (2002). We bootstrap data randomly by shuffling the temporal order of one variable (using blocks of 1-year length) to remove the dependence structure while at the same time preserving seasonality. We repeat this 1 000 times and  $\chi$ , as calculated from the original record, is considered significant if it is greater than 95% of the bootstrapped  $\chi$  estimates (i.e.,  $\alpha=0.05$ ).

To assess time-changing dependence strength,  $\chi$  is calculated using a running time window approach with a 30-year window length (e.g., Hao and Singh, 2020), which is shifted 1 year for each time step. We require at least 25 years of overlapping data in each time window for deriving the metric. Following Wahl et al. (2015), we assess the significance of temporal changes by calculating the range of natural variability. The range of natural variability (10% and 90% levels) is calculated by resampling 30 years of data 10,000 times. The change/variability is significant if the value of  $\chi$  calculated in a time window is outside that range.

#### 2.3. Relating changes in dependence to large-scale climate indices

Our second objective is to investigate the relationships between time-varying dependence strength and large-scale climate indices. For this, we carry out a correlation and significance analysis between eight large-scale climate indices and time-changing  $\chi$  from the non-stationary dependence strength analysis. The steps are as follows.

- From monthly values of the climate indices, we derive annual averages.
- 2. Apply a low-pass filter, following Wahl and Chambers (2016), using a 30-year moving average to allow direct comparison with  $\chi$  calculated using a 30-year moving time window approach.
- 3. Calculate Pearson correlation coefficient between 30-year running  $\chi$  and low-pass filtered climate indices.
- 4. Calculate lag-1 autocorrelation of the 30-year running  $\chi$  time series and low-pass filtered climate indices.
- 5. Calculate significance (at  $\alpha = 0.05$ ) of the correlation derived in step 3 using a *t*-test which accounts for the effective (reduced) number of degrees of freedom (using the results from step 4) stemming from smoothing and autocorrelation similar to Wahl and Chambers (2016) and Rashid and Wahl (2020).

# 2.4. Changes in dependence structure with time

Our third objective is to assess changes in the dependence structures (in addition to dependence strength from the first objective) between different combinations of coastal and inland flooding drivers. Changes in the dependence structure can also lead to changes in joint return periods and in turn design values corresponding to joint return periods even if dependence strength and the marginal distributions of variables remain stationary. To analyse changes in the dependence structure, we use the last 30 years as a reference period and compare it to the data from all other overlapping 30-year time windows. We determine whether the dependence structures differ significantly from each other by comparing the extreme regions of the distributions using the Kullback-Leibler (KL) divergence. The method was introduced by Zscheischler et al. (2021) to investigate if the dependence structure between wind and precipitation extremes was different across different datasets in a study location in Europe. Also, Vignotto et al. (2021) used the KL divergence for clustering bivariate dependencies of compound precipitation and wind extremes over Great Britain and Ireland. In an earlier study, Nasr et al. (2021) used the KL divergence to compare dependence structures of compound flooding drivers derived from observation-based data and model-based data. The method builds on the previous work of Naveau et al. (2014) for comparing univariate datasets and extends it to bivariate (multivariate) datasets.

The methodology here is briefly described but recommend that the reader refers to earlier studies for further details (Nasr et al., 2021; Zscheischler et al., 2021; Vignotto et al., 2021; and references therein for more details). For two bivariate distributions  $X^{(1)} = (X_1^{(1)}, X_2^{(1)})$  and  $X^{(2)} = (X_1^{(2)}, X_2^{(2)})$ , corresponding to bivariate distributions from reference periods (most recent 30 years, X(1)) and sliding 30-year window data (shifted 1 year at a time,  $X^{(2)}$ ), the divergence is only defined in the tail of the distributions after normalizing the marginal distributions to standard Pareto distributions. A risk function (r:  $R^2 \longrightarrow R$ ) calculated on the Pareto scale is used to define extremal regions on each of the bivariate distributions. From the risk functions introduced in Zscheischler et al. (2021) we choose the 'minimum' corresponding to  $r(\mathbf{x}) = \min(x_1, x_2)$ , with  $\mathbf{x} = (x_1, x_2)$  as it covers both asymptotically dependent and independent data. This results in two univariate variables:  $R^{(1)} = r(X^{(1)})$  and  $R^{(2)} = r(X^{(2)})$ . We consider points as extreme when the variable  $R^{(j)}$  exceeds a given high quantile threshold  $q_u^{(j)}$  corresponding to an exceedance probability  $u \in (0,1), j=1,2$ . Varying the threshold  $q_u^{(j)}$  changes the extremal region of interest (we used u = 0.9 to be consistent with the tail dependence threshold we employed in the first objective). Applying the minimum risk function for each of the two bivariate distributions, the extreme points are contained in the set  $\{R^{(j)} > q_u^{(j)}\}, j = 1, 2$ . This set is then divided into a fixed number of disjoint sets  $A_1^{(j)},...,A_W^{(j)}$ . For the minimum risk function the data is split into W = 3 sets where one contains the co-occurring extremes and the other two contain data when only one variable is extreme.

For the two random samples  $(X_1^1,...,X_n^1)$  and  $(X_1^2,...,X_n^2)$  from the two distributions  $X^{(1)}$  and  $X^{(2)}$ , the empirical proportions of data points in each of the previously mentioned sets  $A_w^{(j)}$  are computed as:

$$\widehat{p}_{w}^{(j)} = \frac{\#\left\{i: X_{i}^{(j)} \varepsilon A_{w}^{(j)}\right\}}{\#\left\{i: r\left(X_{i}^{(j)}\right) > q_{u}^{(j)}\right\}}, w = 1, ..., W; j = 1, 2; i = 1, ..., n.$$

The dissimilarity between the extremal behaviours of the two distributions can be accounted for as the KL divergence between the two multinomial distributions defined through the previous empirical proportions as follows:

$$d_{12} = D\left(X_1^{(1)}, X_2^{(1)}\right) = \frac{1}{2} \sum_{w=1}^{W} \left( \left(\widehat{p}_w^{(1)} - \widehat{p}_w^{(2)}\right) \log \left(\frac{\widehat{p}_w^{(1)}}{\widehat{p}_w^{(2)}}\right) \right)$$

The divergence  $d_{12}$  is a way to contrast the differences between extremal dependence structures for asymptotically dependent and independent data. Also, it is symmetric and no additional model assumptions are required as it is a non-parametric statistic. The statistic  $d_{12}$  follows a  $\chi^2(W-1)$  distribution in the limit as the sample size approaches  $\infty$  under suitable assumptions. This allows the estimation of whether it differs significantly from zero.

## 2.5. Non-stationarity in a multivariate statistical framework

In the final step, we perform a complete multivariate statistical analysis between surge and discharge using a 30-year sliding time window for Washington, DC. This location is chosen as it has a long overlapping record of surge and discharge along with a high strength and variability in dependence. The process is explained as follows:

First, using time series of surge (S) and discharge (Q), we apply a peak-over-threshold (POT) approach to obtain independently cluster maxima series for each driver. Second, we use two-way sampling to pair

the peak events of the conditioning variable with largest value of the conditioned variable within 3 days (e.g., Kim et al., 2022). The outcomes are two bivariate samples, one conditioned on S (COS) and the other conditioned on Q (COD). Third, we calculate Kendall's  $\tau$  (Kendall, 1938) for the two samples.

Next, we use the framework by Jane et al. (2020) based on copula theory to derive design events for different return periods (RP) or annual exceedance probabilities (AEPs). First, we fit extreme marginal distributions to the conditioning variables in each of the two samples and non-extreme marginal distributions for the conditioned variables. For the first sample that is (COS) we used a generalized Pareto distribution (GPD) to model S and test a set of distributions for Q that are bounded at zero (e.g., Birnbaum-Saunders, exponential, gamma, lognormal, truncated normal, Tweedie, Weibull, generalized gamma). For the second sample that is (COD) we again use a generalized Pareto distribution (GPD) to model the conditioning variable Q in this case and test unbounded distributions (Gaussian, Logistic) for S. We use the Akike information criterion to select the best distribution (AIC; Akaike, 1974).

After estimation of the extreme and non-extreme marginal distributions, we obtain the copulas that best describe the joint dependence between Q and S. From a range of copula models that can capture different types of dependence structures (upper tail, lower tail, or no tail dependence) we select the best for each of the two samples using AIC. From these copula models, isolines for different joint AEPs can be estimated (Bender et al., 2016). The design event corresponding to the probability that both S and Q exceed the associated values concurrently is expressed as the "AND-Joint Return Period" and is extracted by selecting an event on the isoline. We choose the "AND" hazard scenario since it represents the concurrent occurrence of both extreme events, similar to the recent compound flooding studies (e.g., Jane et al., 2020; Kim et al., 2022; Peña et al., 2023). The selected "most-likely" design event corresponds to the event on the isoline with the highest probability density given the observed data. All calculations are scripted in R Studio (R Core Team, 2020) and the pre-processing and multivariate (bivariate) modelling are conducted with the MultiHazard R package (https://github.com/rjaneUCF/MultiHazard).

We carry out two experiments. In the first experiment, we investigate the effect of changes in the dependence structure (copula and strength) only, by fixing the marginal distributions to those fit based on the entire time series, but the strength of dependence (Kendall's  $\tau$ ) and copula type are calculated separately in each time window. In the second experiment, we introduce the effect of changes in the marginals distributions by calculating the marginals for each time window.

#### 3. Results

#### 3.1. Changes in dependence strength over time

This section describes the results for the first objective which is to characterize and map the change in dependence strength between different flooding drivers at locations around the CONUS coastline with long overlapping records. First, we show the results for the *S*-Q combination and then for the *S*-P combination. For each combination we show results for the whole year and from the seasonal analysis (in the supplement).

Fig. 2 shows the running tail dependence ( $\chi$ ) between S-Q calculated at a threshold of q=0.9 from the 30-year moving time window analysis; results are exemplarily shown for three locations, distributed along the Gulf and east coast: Washington, DC (left column), Fort Pulaski, GA (middle column), and St. Petersburg, FL (right column). The tail dependence in Washington, DC increases between 1950 and the late 1980s, exceeding the lower and upper ranges of the natural variability. This indicates a significant change and increase in the strength from 0.275 to 0.4. This change is mainly driven by the change in the extratropical season supported by their similar temporal pattern. In St. Petersburg, FL the tail dependence has increased over time and exceeded

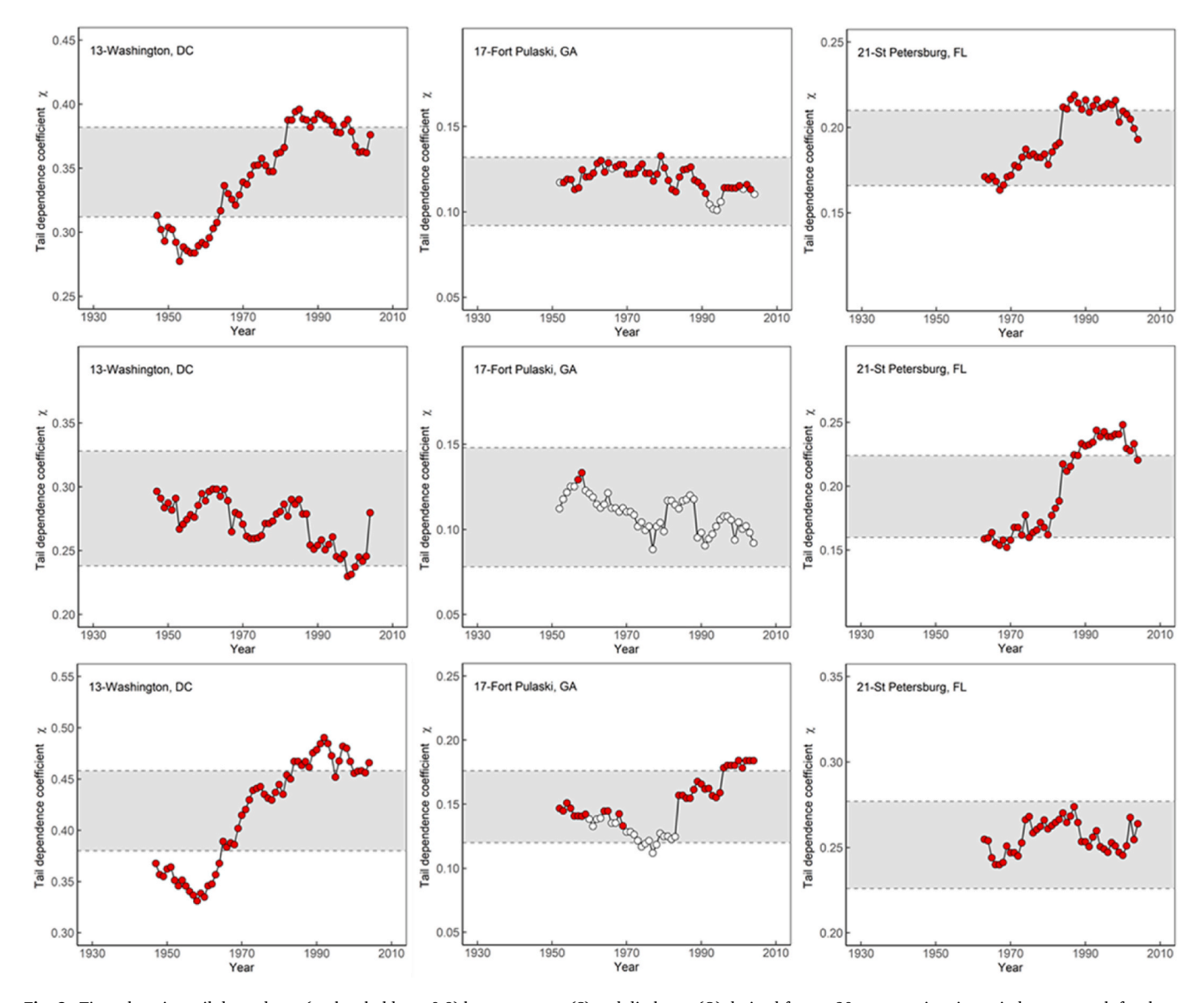


Fig. 2. Time-changing tail dependence (at threshold q=0.9) between surge (S) and discharge (Q) derived from a 30-year moving time window approach for three locations: Washington, DC (left column); Fort Pulaski, GA (middle column); St. Petersburg, FL (right column). Extremal dependence is calculated from the daily timeseries for the entire year (top row), the tropical season (June–November; middle row), and for the extra-tropical season (December–May; bottom row). Each circle represents the midpoint of the 30-year time window. Grey horizontal bands represent the range of natural variability of tail dependence (10% and 90%) from a resampling approach. Red markers indicate significant tail dependence (at  $\alpha=0.05$ ), while non-significant values are marked in white. (For interpretation of the references to colour in this figure legend, the reader is referred to the Web version of this article.)

the range of natural variability in the late 1980s. This increase is also evident during (and driven by) the tropical season where hurricanes and tropical storms in the region often lead to high discharge and surge. In Fort Pulaski, GA the tail dependence is relatively stable over time (i.e., no exceedances of the range of natural variability) when analysing data from the entire year. However, during the extra-tropical season the tail dependence started to increase from the mid-1970s and exceeded the range of natural variability since the early 1990s. Performing this analysis for the entire year and for the different seasons highlights two things. First, if a change occurs in the annual time series, then the seasonal analysis informs which season mainly drives this change (for example in Washington, DC and St. Petersburg, FL). Second, if no change occurs during the entire year, it is still important to investigate changes during different seasons (as in Fort Pulaski, GA) as these may cause changes in flood risk during specific times of the year which are otherwise not captured.

Fig. 3 shows results for changing  $\chi$  between S-Q calculated at a

threshold of q=0.9 for all locations. The mean of each  $\chi$  time series was removed (and is listed in brackets after the respective station name) to better highlight the changes over time. Along the East coast and eastern part of the Gulf of Mexico  $\chi$  was above its mean value for 30-year windows centered in the 1980s and onwards and the range of natural variability was exceeded during that time at various locations. This behaviour is however reversed for the West coast and western part of the Gulf of Mexico. Similar results are found for the tropical (Fig. S1) and extra-tropical (Fig. S2) seasons for the eastern part of the CONUS where  $\chi$  was mostly above mean values for the most recent years while it was below mean values on the West Coast for the same time period.

The same results but for time-changing  $\chi$  between S–P are shown in Fig. 4. For the East and Gulf coasts there is a mixed pattern where some locations are experiencing variability above the mean and others below over the same time period. For the West coast results are more coherent and the variability is below the mean for time windows centered before the mid-1970s, then it becomes larger to reach values above the mean

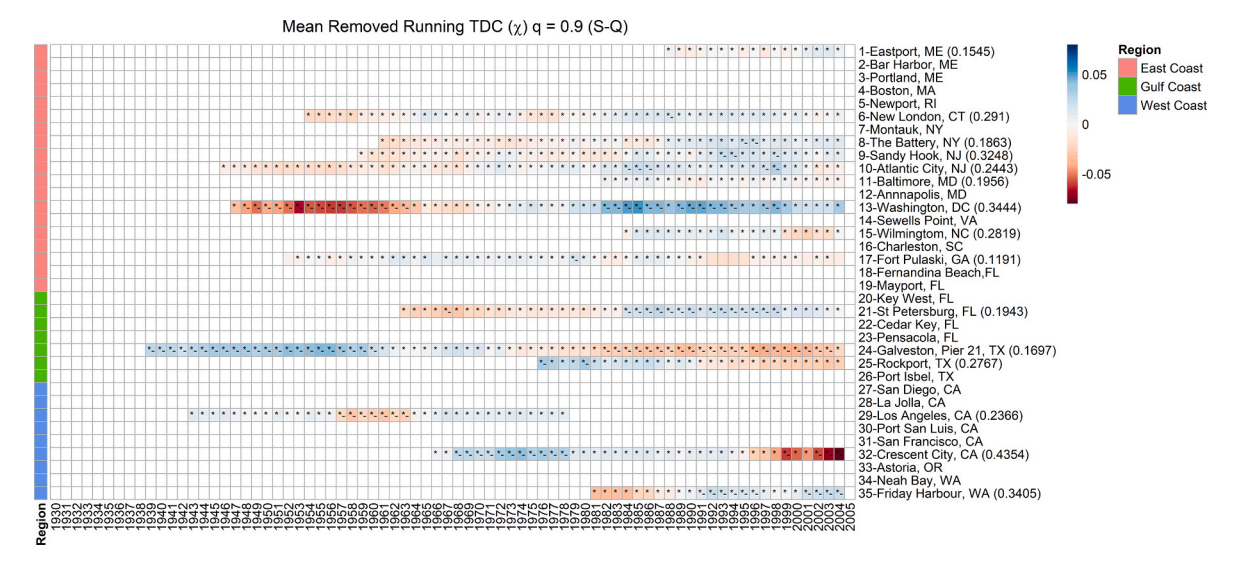


Fig. 3. Heat map showing the changing tail dependence (for threshold q=0.9) for S-Q when using daily data from the entire year; the mean has been removed (tail dependence anomaly) from each time series and the mean values are listed in brackets after the station names. Blank boxes indicate that calculations were not carried out in that box due to lack or insufficiency of available overlapping observations. Asterisk (\*) indicates significant tail dependence (at  $\alpha=0.05$ ) and the hyphen (–) indicates that the value is outside the range of natural variability (10%–90%). Each point represents the midpoint of the 30-year time window.

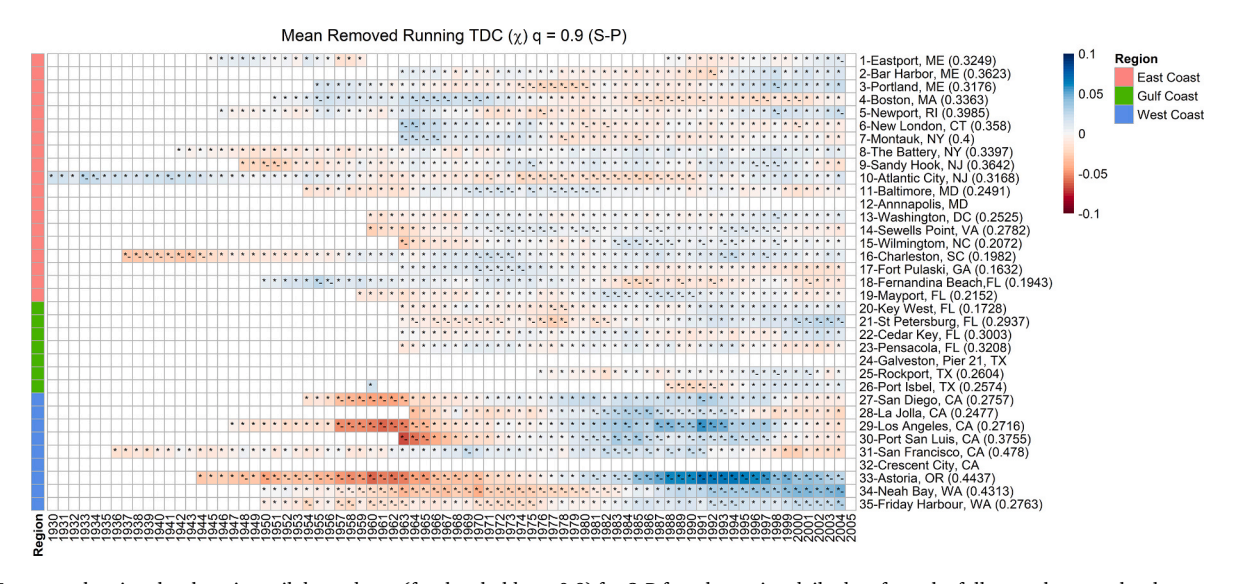


Fig. 4. Heat map showing the changing tail dependence (for threshold q = 0.9) for S-P for when using daily data from the full year; the mean has been removed (tail dependence anomaly) from each time series and the mean values are listed in brackets after the station names. Blank boxes indicate that calculations were not carried out in that box due to lack or insufficiency of available overlapping observations. Asterisk (\*) indicates significant tail dependence (at  $\alpha = 0.05$ ) and the hyphen (-) indicates that the value is outside the range of natural variability (10%–90%). Each point represents the midpoint of the 30-year time window.

and drops again below the mean in the early 2000s at locations in California.

During the tropical season (Fig. S3), the East and Gulf coasts experience variability above the mean for the most recent years. On the other hand, the West coast experiences variability below the mean in California for the most recent years. Stations on the northwest coast in Oregon and Washington experience generally stronger variability during the tropical season, with values consistently below the mean before the 1980s and above the mean afterwards. During the extra-tropical season (Fig. S4) this is reversed and the East and Gulf coasts experience variability below the mean for the most recent years while the West Coast experiences variability above the mean.

On the West coast the variability of *S*–P in the northern part (Oregon and Washington) differs from the southern part (California). The

variability in Oregon and Washington is driven by the variability during summer season (Tropical season) while that of California is driven by variability in the winter season (Extra-tropical season). This is in agreement with the seasonality of rainfall in California as it often experiences heavy rainfall events when atmospheric rivers make landfall during winter as happened recently in January 2023.

## 3.2. Changes in dependence and large-scale climate indices

This section describes the results for the second objective which is to investigate relationships between time-varying dependence strength and large-scale climate indices.

Fig. 5 shows a heat map for Pearson correlation coefficient between time changing  $\chi$  (using a threshold of q=0.9) for S-Q and eight

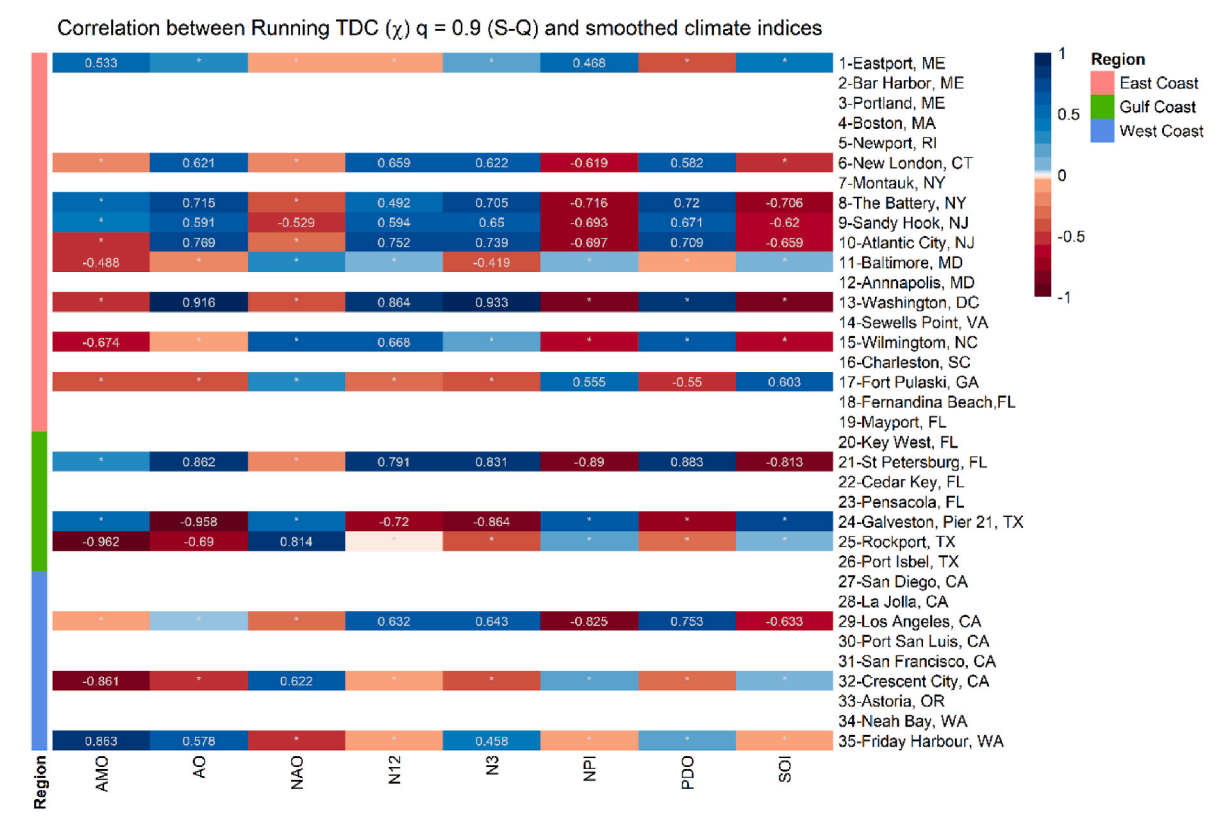


Fig. 5. Heat map for Pearson correlation between time changing tail dependence coefficient  $\chi$  (using a threshold of q=0.9) for S-Q and smoothed climate indices. Numbers indicate significant values (at  $\alpha=0.05$ ) while asterisk (\*) indicates non-significant values.

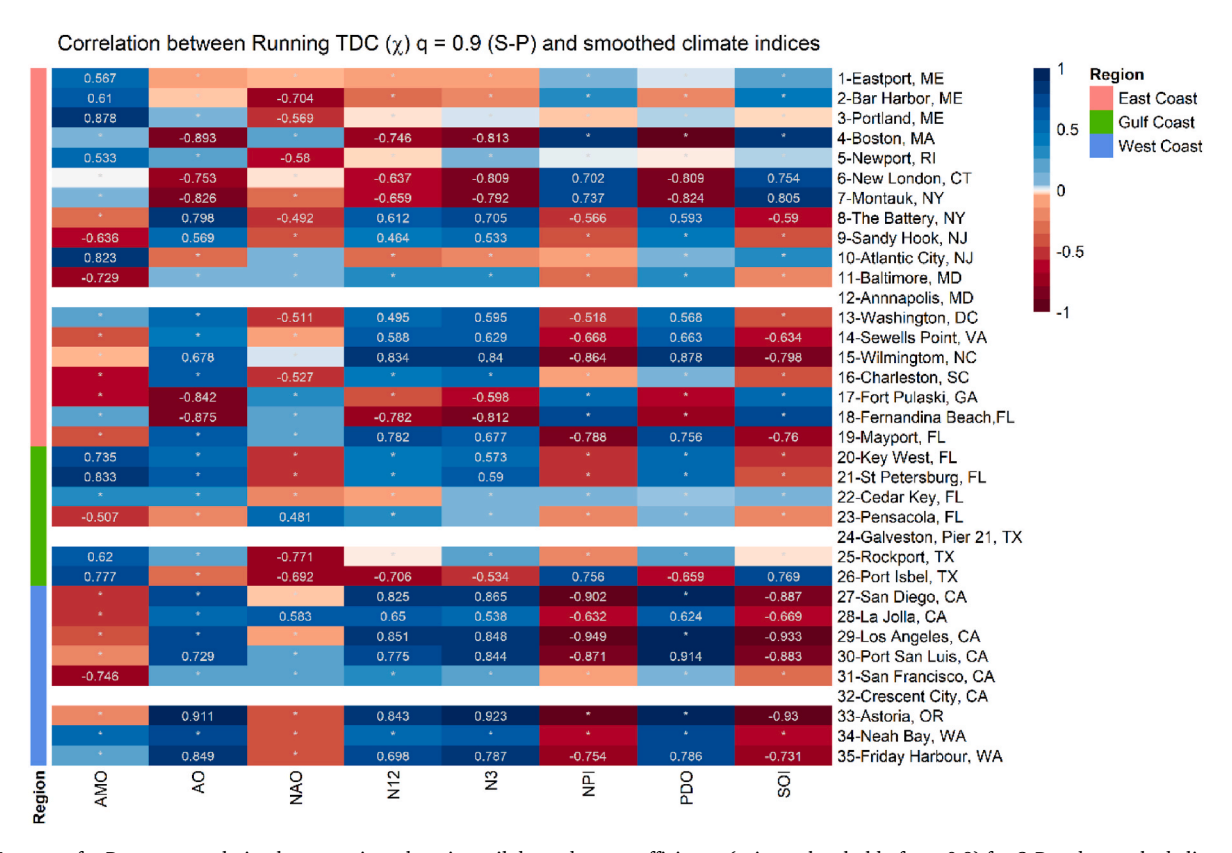


Fig. 6. Heat map for Pearson correlation between time changing tail dependence coefficient  $\chi$  (using a threshold of q=0.9) for S–P and smoothed climate indices. Numbers indicate significant values (at  $\alpha=0.05$ ) while asterisk (\*) indicates non-significant values.

smoothed climate indices. There is significant correlation between the time changing  $\chi$  (using threshold of q=0.9) for  $\emph{S-Q}$  and at least 2 climate indices at each of the analysed locations. The same is found in Fig. 6 for  $\emph{S-P}$ . There is a strong positive correlation in the west coast with the N12, N3, and PDO and negative with NPI and SOI. While it is well-known that oceanic and hydro-meteorological phenomena are influenced by large scale atmospheric circulation, we show here that there is also a strong relationship between changes in dependence (between inland and coastal flooding drivers) and large-scale climate indices.

## 3.3. Changes in dependence structure with time

This section describes the results for the third objective which is to compare the dependence structure (in addition to strength) of different combinations of flooding drivers over time using KL divergence because such changes can also modulate compound flooding potential.

Fig. 7 shows a heatmap for the significance of the KL divergence calculated between the most recent 30-year time window and previous 30-year time windows. Only locations and combinations that showed significant changes in the dependence structure are shown. Unlike the changes in dependence strength, the dependence structure for most locations and variable combinations generally did not change significantly with time. Out of the 12 cases where we find significant changes in the dependence structure, 10 come from the analysis of the S-P variable pair. The locations where the changes occur are mostly located on the west coast; the only location on the east coast with changes in the dependence structure is Washington DC, where it happens for the S-Q (extra-tropical season) and S-Q (full year) cases. We find five cases where changes are significant when the whole (full) year is analysed, four cases where changes occur in the tropical season, and three cases where changes occur in the extra-tropical season. In most cases the changes occurred earlier in the records, while the most recent time windows show the same (or similar) dependence structures as the reference time window (i.e., the most recent 30 years of data); this behaviour is expected since recent time windows share a lot of information with the last time window in our moving window approach.

#### 3.4. Effects of non-stationarity on multivariate design values

Here, as part of our fourth objective, we show results from a full multivariate analysis between surge and discharge using copula theory at Washington, DC. We show the effect of change of dependence strength with time on the most likely design point (first experiment) and the combined effect of changes in the dependence and the marginal distributions (second experiment) on design conditions.

We start by showing the copula types used to model dependence in samples where either surge and discharge is conditioned to be above a high threshold. Fig. 8 shows that the copula type selected to model dependence between extreme surge (above q=0.9) and corresponding discharge (red circles) is the Joe copula for all time windows. The Joe copula has upper tail dependence. The copula type selected to model dependence between extreme discharge (above q=0.9) and corresponding surge (shown in blue points) is most often, but not always, the Joe copula. For some time-windows one of five other copulas is selected, but all of them possess upper tail dependence.

Fig. 9 shows the temporal variation in the dependence strength and the discharge and surge values comprising the most likely design event under the 50-year "AND" joint return period scenario (corresponding to an annual exceedance probability (AEP) of 0.02). In Fig. 9a (top panel) we show how  $\tau$  changes over time when conditioning on discharge (COD) and on surge (COS). For both cases,  $\tau$  increases for windows centered at the 1950s/1960s onwards where the maximum  $\tau$  values during recent years reach double the minimum values seen in the past. Fig. 9b (middle panel) shows the effect of changing dependence strength on surge/discharge values associated with the most likely 50-year return period event while keeping the marginal distributions constant. Note that we also allow the copula type to change, but in all time windows the most likely design point is defined by the case (COD or COS) that is modelled with the Joe copula. The effect is more pronounced in surge (~15 cm increase) compared to discharge, which fluctuates in a relatively small range of values. In Fig. 9c (lower panel) we show the same results but now with temporally varying marginal distributions. The effect of changing the marginals is stronger compared to just changing the dependence strength, leading to increases of the design values of both surge and discharge.

#### 4. Discussion

In this study we have quantified the temporal changes in compound flooding potential that arise from the combination of different coastal and inland flooding drivers. Changes over time are assessed using a 30-year sliding time window of the tail dependence coefficient. The sliding time window approach was applied in several previous studies to assess temporal changes in a range of statistical parameters (e.g., Wahl et al., 2015; Wahl and Chambers, 2016; Rashid et al., 2019; Hao and Singh, 2020; Rashid and Wahl, 2020). We chose the tail dependence coefficient to focus on the case when two variables are extreme, as opposed to conditional sampling (using for example Kendall's  $\tau$ ) when only one variable is extreme and not necessarily the other (e.g., Wahl et al., 2015); this approach is still used here in the final objective to implement the multivariate statistical modelling framework at Washington, DC.

For surge and discharge (S-Q), we find that the value of  $\chi$ , calculated using a 30-year window, was above its mean value for windows centered in the 1980s onward on the East coast and the eastern part of the Gulf of Mexico, with a reverse behaviour for the West coast and western part of

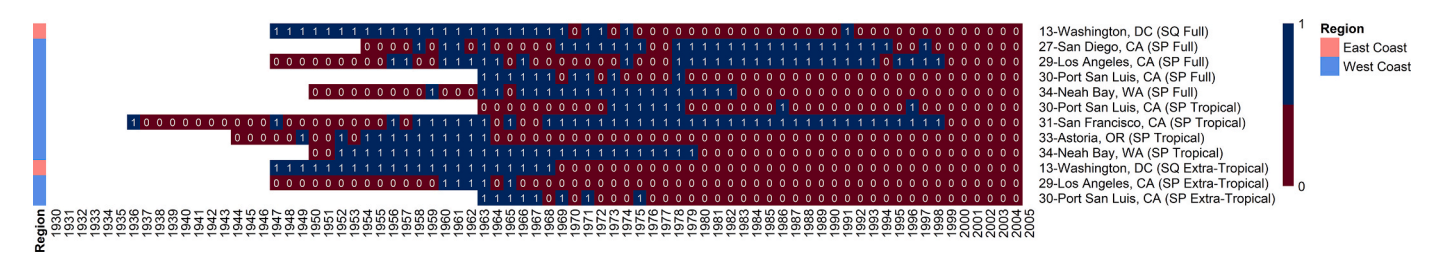


Fig. 7. Heat map for significance of the Kullback–Leibler (KL) divergence between the most recent 30-year and previous 30-year windows. Dark blue (1) indicates significance and dark red (0) indicates non-significance (at  $\alpha = 0.05$ ). (For interpretation of the references to colour in this figure legend, the reader is referred to the Web version of this article.)

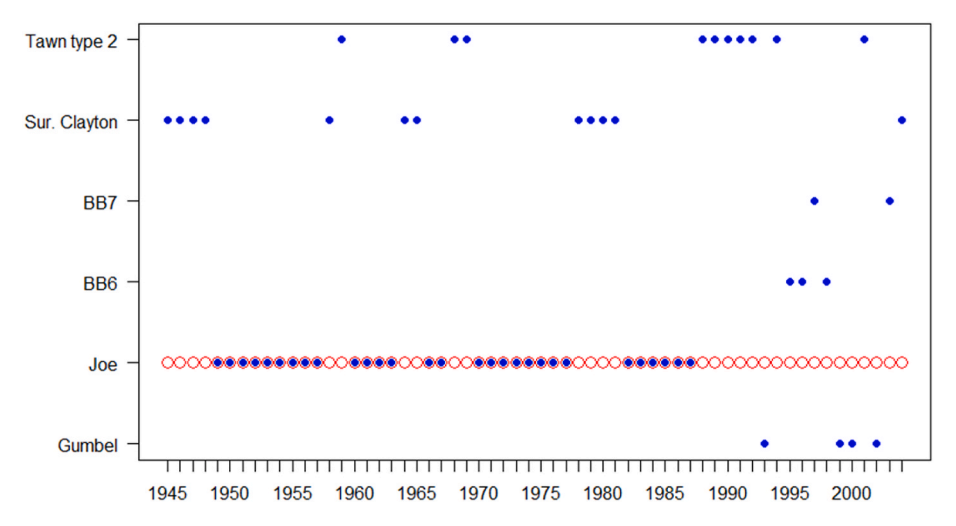


Fig. 8. Best performing copula at Washington DC for the sample containing extreme discharge (above q = 0.9) and corresponding surge (blue points) and for the sample of extreme surge (above q = 0.9) and corresponding discharge (red circle). Each result point is at the center of a 30-year sliding time window. (For interpretation of the references to colour in this figure legend, the reader is referred to the Web version of this article.)

the Gulf of Mexico. This pattern in general is similar for both tropical and extra-tropical seasons.

We find that for S-Q the running  $\chi$  is significantly correlated to at least two climate indices at any given location from the analysed locations. The running  $\chi$  is positively correlated with the low-pass filtered Arctic Oscillation (AO), Niño 1.2 (N12), and Niño 3 (N3) in the East coast and eastern Gulf of Mexico and negatively correlated with the same indices in the western Gulf of Mexico. Using a weather typing approach, Camus et al. (2022) showed positive correlation between the occurrence of compound S-Q events and Niño 3.4, also known as Oceanic Niño Index, for select locations in the East coast and Gulf of Mexico. In case of S-P, in the West coast, the running  $\chi$  is positively correlated with Niño 1.2 (N12), Niño 3 (N3), and Pacific Decadal Oscillation (PDO); and is negatively correlated with North Pacific Index (NPI) and Southern Oscillation Index (SOI).

The spatial distribution in the temporal change of tail dependence was found to be correlated with some large-scale climate indices. These results are not surprising as hydrometeorological and oceanic phenomena are physically connected globally through various excitation mechanisms by atmospheric circulation (Mullon et al., 2013). Some climate indices (e.g., ENSO) are known to influence storminess and occurrence of hurricanes and storms that lead to extreme storm surge and heavy precipitation in a short time. Wahl and Chambers (2016) and Rashid and Wahl (2020) showed how climate indices affect extreme surge levels, whereas in this study, we show that similar relationships also exist between these indices and the dependence between inland and coastal flooding drivers.

Contrary to the change of the dependence strength with time, results from the KL divergence and copula analysis show that the overall dependence structure (i.e., copula type) does not significantly change over time. From the copula analysis results shown for Washington, DC, we find that the strength of dependence, as reflected by Kendall's rank correlation coefficient  $\tau$ , increases with time and this increase in dependence propagates to the increase in potential compound flood hazard when using constant marginals. Changes in the marginal distributions have a much stronger effect than changes in dependence strength on compound flood hazard potential. While the selected copula type is more variable when analysing the sample conditions on discharge (Fig. 8), we note that all copulas that are selected for the different time windows have upper tail dependence; hence the overall impact on the joint probabilities is still relatively small. Overall, these findings are in agreement with other studies (e.g., Bender et al., 2014; Hao and Singh, 2020; Razmi et al., 2022). However, those were all individual case studies, and it is still important for non-stationary compound flood assessments to account for potential changes in dependence strength (and structure) as an additional source of non-stationarity.

Finally, we acknowledge that while our observational database is very good in comparison to many other studies for other parts of the world, it's still limited, especially for the purpose of assessing non-stationarity. As has been shown, for example, in Santos et al. (2021a), natural climate variability can lead to changes in compound flood potential at multi-decadal time scales. Hence, the results presented here should not be interpreted as emerging long-term trends because of climate change, but rather show where and how much compound flood potential has varied in the past. In the same context, Bevacqua et al. (2023) highlight the advantage of integrating ensemble simulations into studies of compound weather extremes, including compound flooding, to better understand physical processes connections, assess high-impact low-probability events, and conduct climate attribution studies.

Flood risk generally involves different components: hazard, exposure, and vulnerability. While our focus here was on assessing the hazard component and how it changes with time, it is worth noting that the other components are dynamic as well. Socioeconomic development translates to changes in exposure and vulnerability which increases impacts even when the dependence and marginal distributions of drivers considered are stationary (hazard is stationary). A next step could be to focus on local communities and explore how compound flood risk has evolved with time incorporating hazard, exposure, and vulnerability (e. g., Sebastian et al., 2019).

## 5. Conclusions

We have quantified the temporal variability in compound flooding potential that arises from the combination of storm surge, precipitation, and river discharge along the CONUS coastline. Our first objective was to characterize and map the change in dependence strength between different drivers at locations around the CONUS coastline with long overlapping records. We carried out the analysis at 34 sites, where long enough overlapping datasets with at least 55 years were available for the different variables. We found for S-Q that from 1980 onwards the variability of  $\chi$  was above the mean for the East coast and eastern Gulf of Mexico and below it for the West coast and western Gulf of Mexico.

Our second objective was to investigate whether a statistically significant link between time-varying dependence strength and large-scale climate indices exists. We found high significant correlations between

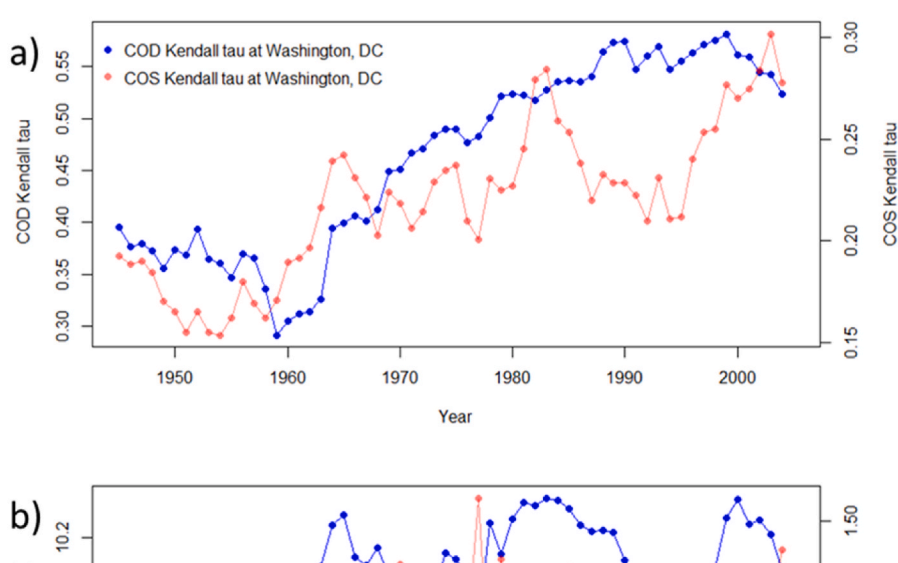
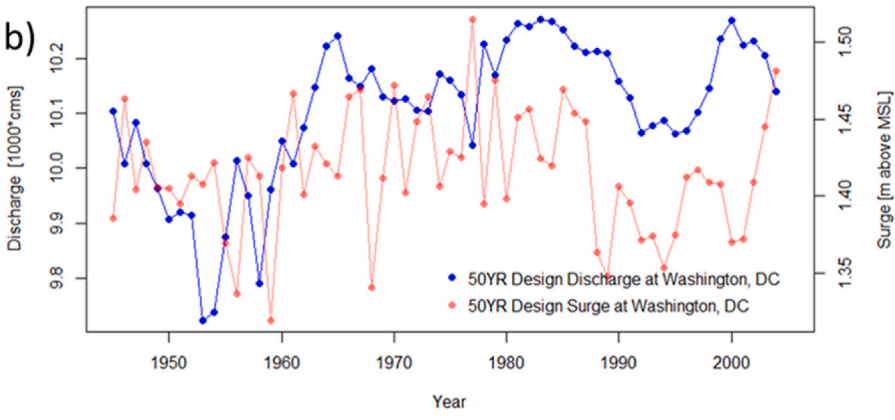
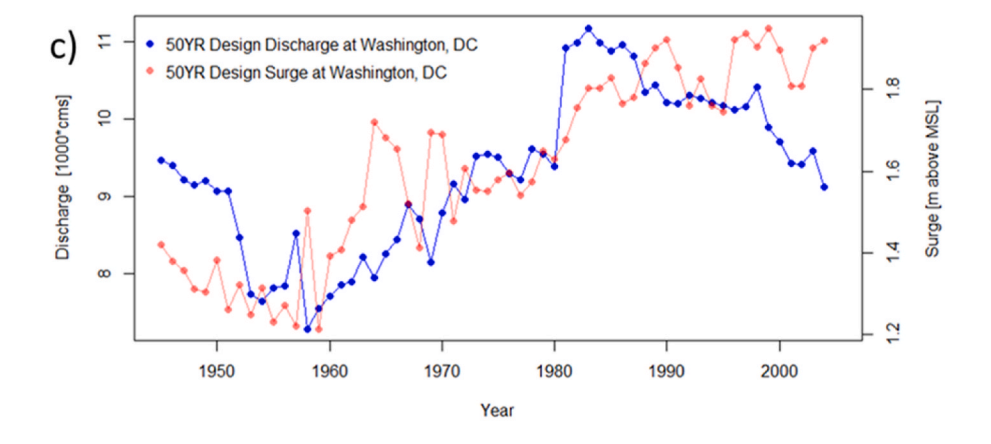


Fig. 9. Dependence strength and surge/discharge values associated with most likely design events at Washington DC calculated using a 30-year sliding time window. Top panel (a) shows Kendall's rank correlation coefficient when conditioning on discharge (COD) and on surge (COS). Middle panel (b) shows surge/discharge values for most-likely 50-year return period events and their changes over time due to varying dependence strength. Bottom panel (c) is the same as (b) but with time varying marginal distributions.





running  $\chi$  and various climate indices (e.g., AO, ENSO, NPI, PDO, and SOI). Changes in  $\chi$  are correlated and linked with large scale atmospheric circulations which modulate hydro-meteorological and ocean-ographic phenomena.

Our third objective was to compare the dependence structures (in addition to strength) of different combinations of flooding drivers over time. Unlike the dependence strength that significantly changes over time, we found no significant change in dependence structure (i.e., copula type that models dependence). Our fourth objective was to perform a complete multivariate analysis for *S*-Q at Washington, DC as an example. We found that the effect of increasing the dependence strength, assuming stationary marginal distributions, is more pronounced for surge than discharge which is translated to a potential

increase in coastal flood hazard compared to fluvial flood hazard. Varying the marginals with time in addition to the dependence leads to a significant increase in discharge and surge associated with most-likely 50-year return period events.

Our study focuses on temporal changes of the dependence which is part of the hazard component of potential compound flood risk. Flood risk is non-stationary as it involves changes in hazard, exposure, and vulnerability components over time. Incorporating these changes can lead to better understanding of flood risk in the future, leading to better planning that results into increasing resilience of coastal communities.

#### 6. Code availability

Data pre-processing, analysis and visualization were carried out in R programming language (R Core Team, 2020). The following R packages were used: 'dataRetrieval' (De Cicco et al., 2018) and 'rnoaa' (Chamberlain et al., 2016) for data retrieval; 'dplyr' (Wickham et al., 2020b), 'lubridate' (Spinu et al., 2020), and 'tidyr' (Wickham, 2020) for data pre-processing. 'ExtRemes' (Gilleland and Katz, 2016), 'MultiHazard' (Jane et al., 2020), and other routines for data analysis; and 'ggplot2' (Wickham et al., 2020a) and 'pheatmap' (Kolde, 2015) for visualization.

## **Author contributions**

AAN and TW conceived the study. AAN performed the analysis and wrote the first draft of the paper. RJ developed the MultiHazard R Package used for the bivariate modelling. IDH, PC, RAJ and MMR participated in technical discussions. All authors revised and co-wrote the paper.

## Financial support

This material is based upon work supported by the National Science Foundation (NERC-NSF joint funding opportunity) under NSF Grant Number 1929382 (TW and AAN). PC and IDH's time on this research have been supported by the United Kingdom NERC grant CHANCE (grant no. NE/S010262/1). TW also acknowledges support by the USACE Climate Preparedness and Resilience Community of Practice and Programs.

#### **Author statement**

Ahmed A. Nasr: Conceptualization, Methodology, Software, Validation, Formal Analysis, Investigation, Data Curation, Visualization, Writing - Original Draft, Writing - Review & Editing. Thomas Wahl: Conceptualization, Methodology, Resources, Writing - Review & Editing, Supervision, Project Administration, Funding Acquisition. Md Mamunur Rashid: Writing - Review & Editing. Robert A. Jane: Software, Writing - Review & Editing. Paula Camus: Writing - Review & Editing. Ivan D. Haigh: Writing - Review & Editing.

# Declaration of competing interest

The authors declare that they have no known competing financial interests or personal relationships that could have appeared to influence the work reported in this paper.

# Data availability

Links to data and codes used are specified in the text and included in the data and code availability sections at the end of teh manuscript

#### Acknowledgements

We thank Jakob Zscheischler and Philippe Naveau for making their code available to apply the KL divergence method.

## Appendix A. Supplementary data

Supplementary data to this article can be found online at  $\frac{https:}{doi.}$  org/10.1016/j.wace.2023.100594.

#### References

Akaike, H., 1974. New look at statistical-model identification. IEEE Trans. Automat. Control 19, 716–723. https://doi.org/10.1109/tac.1974.1100705.

- Bender, J., Wahl, T., Jensen, J., 2014. Multivariate design in the presence of nonstationarity. J. Hydrol. 514, 123–130. https://doi.org/10.1016/j. ibudea.12014.04.017
- Bender, J., Wahl, T., Müller, A., Jensen, J., 2016. A multivariate design framework for river confluences. Hydrol. Sci. J. 61, 471–482. https://doi.org/10.1080/ 02626667.2015.1052816.
- Bevacqua, E., Maraun, D., Hobæk Haff, I., Widmann, M., Vrac, M., 2017. Multivariate statistical modelling of compound events via pair-copula constructions: analysis of floods in Ravenna (Italy). Hydrol. Earth Syst. Sci. 21, 2701–2723. https://doi.org/ 10.5194/hess-21-2701-2017.
- Bevacqua, E., Vousdoukas, M.I., Shepherd, T.G., Vrac, M., 2020. Brief communication: the role of using precipitation or river discharge data when assessing global coastal compound flooding. Nat. Hazards Earth Syst. Sci. 20, 1765–1782. https://doi.org/ 10.5194/nhess-20-1765-2020.
- Bevacqua, E., Suarez-Gutierrez, L., Jézéquel, A., Lehner, F., Vrac, M., Yiou, P., Zscheischler, J., 2023. Advancing research on compound weather and climate events via large ensemble model simulations. Nat. Commun. 14, 2145. https://doi.org/ 10.1038/s41467-023-37847-5.
- Bromirski, P.D., Flick, R.E., Cayan, D.R., 2003. Storminess variability along the California coast: 1858–2000. J. Clim. 16, 982–993. https://doi.org/10.1175/1520-0442(2003)016<0982:SVATCC>2.0.CO;2.
- Bromirski, P.D., Flick, R.E., Miller, A.J., 2017. Storm surge along the Pacific coast of North A merica. J. Geophys. Res. Oceans. 122, 441–457. https://doi.org/10.1002/ 2016JC012178.
- Camelo, J., Mayo, T.L., Gutmann, E.D., 2020. Projected climate change impacts on hurricane storm surge inundation in the coastal United States. Front. Built Environ. 6, 588049 https://doi.org/10.3389/fbuil.2020.588049.
- Camus, P., Haigh, I.D., Nasr, A.A., Wahl, T., Darby, S.E., Nicholls, R.J., 2021. Regional analysis of multivariate compound coastal flooding potential around Europe and environs: sensitivity analysis and spatial patterns. Nat. Hazards Earth Syst. Sci. 21, 2021–2040. https://doi.org/10.5194/nhess-21-2021-2021.
- Camus, P., Haigh, I.D., Wahl, T., Nasr, A.A., Méndez, F.J., Darby, S.E., Nicholls, R.J., 2022. Daily synoptic conditions associated with occurrences of compound events in estuaries along North Atlantic coastlines. Int. J. Climatol. 42, 5694–5713. https:// doi.org/10.1002/joc.7556.
- Chamberlain, S., Anderson, B., Salmon, M., Erickson, A., Potter, N., Stachelek, J., Simmons, A., Ram, K., Edmund, H., 2016. rnoaa: NOAA weather data from R. CRAN. https://CRAN.R-project.org/package=rnoaa.
- Codiga, D.L., 2011. Technical report 2011-01. In: Unified Tidal Analysis and Prediction Using the UTide Matlab Functions. Graduate School of Oceanography, University of Rhode Island, Narragansett. 1–59, available at: http://www.po.gso.uri.edu/pub/downloads/codiga/pubs/2011Codiga-UTide-Report.pdf. (Accessed 25 June 2020).
- Couasnon, A., Sebastian, A., Morales-Nápoles, O., 2018. A copula-based bayesian Network for modeling compound flood hazard from riverine and coastal interactions at the catchment scale: an application to the houston ship channel. Texas. Water 10, 1190. https://doi.org/10.3390/w10091190.
- Couasnon, A., Eilander, D., Muis, S., Veldkamp, T.I.E., Haigh, I.D., Wahl, T., Winsemius, H.C., Ward, P.J., 2020. Measuring compound flood potential from river discharge and storm surge extremes at the global scale and its implications for flood hazard. Nat. Hazards Earth Syst. Sci. 20, 489–504. https://doi.org/10.5194/nhess-20.489.2020.
- De Cicco, L.A., Lorenz, D., Hirsch, R.M., Watkins, W., 2018. dataRetrieval: R Package for Discovering and Retrieving Water Data available from: U.S. federal hydrologic web services. CRAN. https://CRAN.R-project.org/package=dataRetrieval.
- Gilleland, E., Katz, R.W., 2016. Extremes 2.0: an extreme value analysis package in R. J. Stat. Software 72, 1–39. https://doi.org/10.18637/jss.v072.i08.
- Gori, A., Lin, N., Xi, D., Emanuel, K., 2022. Tropical cyclone climatology change greatly exacerbates US extreme rainfall-surge hazard. Nat. Clim. Change 12, 171–178. https://doi.org/10.1038/s41558-021-01272-7.
- Hanson, S., Nicholls, R., Ranger, N., Hallegatte, S., Corfee-Morlot, J., Herweijer, C., Chateau, J., 2011. A global ranking of port cities with high exposure to climate extremes. Climatic Change 104, 89–111. https://doi.org/10.1007/s10584-010-9977-4.
- Hao, Z., Singh, V.P., 2020. Compound events under global warming: a dependence perspective. J. Hydrol. Eng. – ASCE 25, 03120001. https://doi.org/10.1061/(ASCE) HE.1943-5584.0001991.
- Hendry, A., Haigh, I.D., Nicholls, R.J., Winter, H., Neal, R., Wahl, T., Joly-Laugel, A., Darby, S.E., 2019. Assessing the characteristics and drivers of compound flooding events around the UK coast. Hydrol. Earth Syst. Sci. 23, 3117–3139. https://doi.org/ 10.5194/hess-23-3117-2019.
- Jane, R., Cadavid, L., Obeysekera, J., Wahl, T., 2020. Multivariate statistical modelling of the drivers of compound flood events in south Florida. Nat. Hazards Earth Syst. Sci. 20, 2681–2699. https://doi.org/10.5194/nhess-20-2681-2020.
- Jane, R., Wahl, T., Santos, V.M., Misra, S.K., White, K.D., 2022. Assessing the potential for compound storm surge and extreme river discharge events at the catchment scale with statistical models: sensitivity analysis and recommendations for best Practice. J. Hydrol. Eng. 27, 04022001 https://doi.org/10.1061/(ASCE)HE.1943-5584 0002154
- Kendall, M.G., 1938. A new measure of rank correlation. Biometrika 30, 81–93. https://doi.org/10.2307/2332226.
- Kennedy, A.J., Griffin, M.L., Morey, S.L., Smith, S.R., O'Brien, J.J., 2007. Effects of El niño-southern oscillation on sea level anomalies along the Gulf of Mexico coast. J. Geophys. Res. Oceans. 112, C05047 https://doi.org/10.1029/2006JC003904.
- Kew, S.F., Selten, F.M., Lenderink, G., Hazeleger, W., 2013. The simultaneous occurrence of surge and discharge extremes for the Rhine delta. Nat. Hazards Earth Syst. Sci. 13, 2017–2029. https://doi.org/10.5194/nhess-13-2017-2013.

- Kim, H., Villarini, G., Jane, R., Wahl, T., Misra, S., Michalek, A., 2022. On the generation of high-resolution probabilistic design events capturing the joint occurrence of rainfall and storm surge in coastal basins. Int. J. Climatol. 1–11. https://doi.org/ 10.1002/joc.7825.
- Kolde, R., 2015. pheatmap: pretty heatmaps in R. CRAN. https://CRAN.R-project.org/package=pheatmap.
- Ledford, A.W., Tawn, J.A., 1997. Modelling dependence within joint tail regions. J. Roy. Stat. Soc. B 59, 475–499. https://doi.org/10.1111/1467-9868.00080.
- Marcos, M., Rohmer, J., Vousdoukas, M., Mentaschi, L., Le Cozannet, G., Amores, A., 2019. Increased extreme coastal water levels due to the combined action of storm surges and wind-waves. Geophys. Res. Lett. 1 https://doi.org/10.1029/ 2019GL082599, 2019GL082599.
- Moftakhari, H.R., Salvadori, G., AghaKouchak, A., Sanders, B.F., Matthew, R.A., 2017. Compounding effects of sea level rise and fluvial flooding. P. Natl. Acad. Sci. USA. 114, 9785–9790. https://doi.org/10.1073/pnas.1620325114.
- Mullon, L., Chang, N.B., Yang, Y.J., Weiss, J., 2013. Integrated remote sensing and wavelet analyses for screening short-term teleconnection patterns in northeast America. J. Hydrol. 499, 247–264. https://doi.org/10.1016/j.jhydrol.2013.06.046.
- Naseri, K., Hummel, M., 2022. A bayesian copula-based nonstationary framework for compound flood risk assessment along US coastlines. J. Hydrol. 610, 128005 https:// doi.org/10.1016/j.jhydrol.2022.128005.
- Nasr, A.A., Wahl, T., Rashid, M.M., Camus, P., Haigh, I.D., 2021. Assessing the dependence structure between oceanographic, fluvial, and pluvial flooding drivers along the United States coastline. Hydrol. Earth Syst. Sci. 25, 6203–6222. https:// doi.org/10.5194/hess-25-6203-2021.
- Naveau, P., Guillou, A., Rietsch, T., 2014. A non-parametric entropybased approach to detect changes in climate extremes. J. Roy. Stat. Soc. B 76, 861–884. https://www. istor.org/stable/24774606.
- NOAA Office for Coastal Management. Economics and demographics. https://coast.noaa.gov/states/fast-facts/economics-and-demographics.html. (Accessed 20 February 2021).
- Paprotny, D., Vousdoukas, M.I., Morales-Nápoles, O., Jonkman, S.N., Feyen, L., 2020.
  Pan-European hydrodynamic models and their ability to identify compound floods.
  Nat. Hazards 101, 933–957. https://doi.org/10.1007/s11069-020-03902-3.
- Peña, F., Obeysekera, J., Jane, R., Nardi, F., Maran, C., Cadogan, A., de Groen, F., Melesse, A., 2023. Investigating compound flooding in a low elevation coastal karst environment using multivariate statistical and 2D hydrodynamic modeling. Weather Clim. Extrem. 39, 100534 https://doi.org/10.1016/j.wace.2022.100534.
- R Core Team, 2020. R: a language and environment for statistical computing. R Foundation Statist. Comput. https://www.R-project.org.
- Rashid, M.M., Wahl, T., Chambers, D.P., Calafat, F.M., Sweet, W.V., 2019. An extreme sea level indicator for the contiguous United States coastline. Sci. Data 6, 1–14. https://doi.org/10.1038/s41597-019-0333-x.
- Rashid, M.M., Wahl, T., 2020. Predictability of extreme sea level variations along the US coastline. J. Geophys. Res. Oceans. 125, e2020JC016295 https://doi.org/10.1029/2020JC016295
- Razmi, A., Mardani-Fard, H.A., Golian, S., Zahmatkesh, Z., 2022, 2022. Time-varying univariate and bivariate frequency analysis of nonstationary extreme sea level for New York City. Environ. Process. 9, 8. https://doi.org/10.1007/s40710-021-00553-
- Rueda, A., Camus, P., Tomás, A., Vitousek, S., Méndez, F.J., 2016. A multivariate extreme wave and storm surge climate emulator based on weather patterns. Ocean Model. 104, 242–251. https://doi.org/10.1016/j.ocemod.2016.06.008.
- Santos, V.M., Casas-Prat, M., Poschlod, D., Ragno, E., van den Hurk, B., Hao, Z., Kalmár, T., Zhu, L., Najafi, H., 2021a. Statistical modelling and climate variability of compound surge and precipitation events in a managed water system: a case study in The Netherlands. Hydrol. Earth Syst. Sci. 25, 3595–3615. https://doi.org/10.5194/ hess-25-3595-2021.

- Santos, V.M., Wahl, T., Jane, R.A., Misra, S.K., White, K.D., 2021b. Assessing compound flooding potential with multivariate statistical models in a complex estuarine system under data constraints. J. Flood Risk Manag, e12749. https://doi.org/10.1111/ifr3.12749
- Sebastian, A., Gori, A., Blessing, R.B., van der Wiel, K., Bass, B., 2019. Disentangling the impacts of human and environmental change on catchment response during Hurricane Harvey. Environ. Res. Lett. 14, 124023 https://doi.org/10.1088/1748-9326/ab5234.
- Serafin, K.A., Ruggiero, P., 2014. Simulating extreme total water levels using a time-dependent, extreme value approach. J. Geophys. Res. Ocean. 119, 6305–6329. https://doi.org/10.1002/2014JC010093.
- Smith, A.B., 2020. U.S. Billion-Dollar Weather and Climate Disasters, 1980 Present (NCEI Accession 0209268). [inland Floods and Tropical Cyclones]. NOAA National Centers for Environmental Information. Dataset. https://doi.org/10.25921/stkw-7w73. (Accessed 20 February 2021).
- Spinu, V., Grolemund, G., Wickham, H., 2020. lubridate: make dealing with dates a little easier R package. CRAN. https://CRAN.R-project.org/package=lubridate.
- Svensson, C., Jones, D.A., 2002. Dependence between extreme sea surge, river flow and precipitation in eastern Britain. Int. J. Climatol. 22, 1149–1168. https://doi.org/ 10.1002/joc.794.
- Tabari, H., 2020. Climate change impact on flood and extreme precipitation increases with water availability. Sci. Rep. 10, 13768 https://doi.org/10.1038/s41598-020-70816-2.
- Wahl, T., Jain, S., Bender, J., Meyers, S.D., Luther, M.E., 2015. Increasing risk of compound flooding from storm surge and rainfall for major US cities. Nat. Clim. Change 5, 1093–1097. https://doi.org/10.1038/nclimate2736.
- Vignotto, E., Engelke, S., Zscheischler, J., 2021. Clustering bivariate dependences in the extremes of climate variables. Weather Clim. Extrem. 32, 100318 https://doi.org/ 10.1016/j.wace.2021.100318.
- Wahl, T., Chambers, D.P., 2016. Climate controls multidecadal variability in US extreme sea level records. J. Geophys. Res. Oceans. 121, 1274–1290. https://doi.org/ 10.1002/2015JC011057.
- Ward, P.J., Couasnon, A., Eilander, D., Haigh, I.D., Hendry, A., Muis, S., Veldkamp, T.I. E., Winsemius, H.C., Wahl, T., 2018. Dependence between high sea-level and high river discharge increases flood hazard in global deltas and estuaries. Environ. Res. Lett. 13. 084012 https://doi.org/10.1088/1748-9326/aad400.
- Wickham, H., 2020. Tidyr: tidy messy data R package. CRAN. https://CRAN.R-project. org/package=tidyr.
- Wickham, H., Chang, W., Henry, L., Pedersen, T.L., Takahashi, K., Wilke, C., Woo, K., Yutani, H., Dunnington, D., 2020a. ggplot2: Create Elegant Data Visualisations Using the Grammar of Graphics R Package. CRAN[code]. https://CRAN.R-project.org/package=ggplot2.
- Wickham, H., Francois, R., Henry, L., Müller, K., 2020b. dplyr: a grammar of data manipulation R Package. CRAN. https://CRAN.R-project.org/package=dplyr.
- Zscheischler, J., Westra, S., van den Hurk, B.J.J.M., Seneviratne, S.I., Ward, P.J., Pitman, A., AghaKouchak, A., Bresch, D.N., Leonard, M., Wahl, T., Zhang, X., 2018. Future climate risk from compound events. Nat. Clim. Change 8, 469–477. https://doi.org/10.1038/s41558-018-0156-3
- Zscheischler, J., Martius, O., Westra, S., Bevacqua, E., Raymond, C., Horton, R.M., van den Hurk, B., Agha Kouchak, A., Jézéquel, A., Mahecha, M.D., Maraun, D., Ramos, A. M., Ridder, N., Thiery, W., Vignotto, E., 2020. A typology of compound weather and climate events. Nat. Rev. Earth Environ. 1, 333–347. https://doi.org/10.1038/s43017-020-0060-z.
- Zscheischler, J., Naveau, P., Martius, O., Engelke, S., Raible, C.C., 2021. Evaluating the dependence structure of compound precipitation and wind speed extremes. Earth Syst. Dynam. 12, 1–16. https://doi.org/10.5194/esd-12-1-2021.